0026-895X/06/6903-718–726$20.00
MOLECULAR PHARMACOLOGY
Copyright © 2006 The American Society for Pharmacology and Experimental Therapeutics
Mol Pharmacol 69:718–726, 2006

Vol. 69, No. 3
18663/3085832
Printed in U.S.A.

1,4-Diazabicyclo[2.2.2]octane Derivatives: A Novel Class of Voltage-Gated Potassium Channel Blockers

Earl Gordon, Jaime-Lee Cohen, Robert Engel, and Geoffrey W. Abbott

Greenberg Division of Cardiology, Department of Medicine and Department of Pharmacology, Weill Medical College, Cornell University, New York, New York (E.G., G.W.A.); Department of Chemistry and Physical Science, Pace University, New York, New York (J.-L.C.); and Department of Chemistry and Biochemistry, Queens College of the City University of New York, Flushing, New York (R.E.)

Received September 3, 2005; accepted November 29, 2005

ABSTRACT

Voltage-gated potassium (Kv) channels are targets for therapeutic drugs in the treatment of pathologic conditions including cardiac arrhythmia and epilepsy. In this study, we synthesized three classes of novel polyammonium compounds incorporating the bicyclic unit 1,4-diazabicyclo[2.2.2]octane (DABCO) and tested their action on three representative mammalian Kv channels (Kv2.1, Kv3.4, and Kv4.2) expressed in *Xenopus laevis* oocytes. Nonsubstituted DABCO did not block the Kv channels tested. Simple DABCO monostrings and diDABCO strings inhibited Kv2.1 and Kv3.4 channels, with potency increasing with string length for both these DABCO classes. Both Kv2.1 and Kv3.4 were most sensitive to C_{16} monostrings, with IC_{50} values of 1.9 and 0.6 μM, respectively. For compounds comprising two DABCO groups separated by an aromatic ring, inhibition depended upon relative positioning of the two DABCO groups, and only the *para* form (JC638.2α) was active, blocking Kv2.1 with an IC_{50} of 186 μM. Kv4.2 channels were relatively insensitive to all compounds tested. Unlike the tetraethylammonium ion (TEA), neither JC638.2α nor C_{16} monostring TA279 produced block when applied intracellularly via the recording electrode to Kv2.1 channels expressed in Chinese hamster ovary cells, suggesting against an internal site of action. However, JC638.2α protected an introduced cysteine (K356C) in the Kv2.1 outer pore from permanent modification by methanethiosulfonate ethyltrimethylammonium (MTSET). These data suggest that JC638.2α occupies an external binding site similar to that of TEA in the Kv2.1 outer pore, but with much higher affinity than TEA. These DABCO salts represent a new class of Kv channel blockers, some with higher potencies than any previously described quaternary ammonium ions. The potential for synthesis of an array of modular derivatives suggests that DABCO compounds hold promise as probes of Kv channel structure and identity and as potential therapeutic agents.

Ion channels regulate fluid homeostasis, electrical excitability, and signal transduction. Voltage-gated potassium (Kv) channels open in response to cellular depolarization to repolarize the cell membrane by allowing efflux of potassium ions at rates approaching the diffusion limit (MacKinnon, 2003). Kv channels consist of tetramers of α subunits, each with six transmembrane α-helical domains (S1–S6), and a pore region. S4 contains basic residues and provides the charge for voltage-sensing; S5–S6 line the conduction pathway and contribute to gating movements (Doyle et al., 1998; Perozo, 2002; Yellen, 2002; Long et al., 2005a,b). A broad, dynamic spectrum of repolarization rates, translating into a variety of action potential profiles, is required, depending on cell type and required function at specific times (Rudy et al., 1999). The biophysical properties of distinct channels, such as the conductance, and voltage dependence and kinetics of gating, are governed by the particular attributes of their component subunits, as well as extrinsic factors such as trafficking, regulation by ancillary subunits, and cellular metabolic state (Gulbis, 2002; MacKinnon, 2003; McCrossan and Abbott, 2004; Heusser and Schwappach, 2005).

Different homomeric α-subunit K^+ channels are highly variable in their sensitivity to blockade by tetraethylammonium ion (TEA), a canonical pore-blocking quaternary ammonium ion. Variation in Kv channel α-subunit sensitivity to externally applied TEA has been attributed to one externally exposed residue near the selectivity filter, position 449 in *Shaker* (position 82 in KcsA; position 380 in Kv2.1). If an aromatic residue occupies this position, TEA affinity is reportedly high (MacKinnon and Yellen, 1990). This was first proposed to result from cation-π orbital interactions but later

G.W.A. was supported by American Heart Association grant 0235069N and National Institutes of Health grant R03-DC07060 and R01-HL079275.
Article, publication date, and citation information can be found at http://molpharm.aspetjournals.org.
doi:10.1124/mol.105.018663.

ABBREVIATIONS: TEA, tetraethylammonium; MTSET, methanethiosulfonate ethyltrimethylammonium; DABCO, 1,4-diazabicyclo[2.2.2]octane; CHO, Chinese hamster ovary; TEVC, two-electrode voltage-clamp; ANOVA, analysis of variance.

suggested to arise from differences in the hydration state of TEA (Crouzy et al., 2001). In a more recent study, however, an external binding site more distal to the selectivity filter was proposed, based on the ability of TEA to protect a cysteine introduced at position 356 in Kv2.1 from modification by methanethiosulfonate ethyltrimethylammonium (MTSET), which normally manifests as permanent channel block (Andalib et al., 2004).

Given the utility of tetraethylammonium salts in the investigation of Kv channel structure and function, we postulated that an organic cation that was permissive to addition of distinct classes of numerous, closely-related small molecules would provide an excellent substrate for the construction of multiple libraries of Kv channel probes. The bicyclic molecule 1,4-diazabicyclo[2.2.2]octane (DABCO) is a convenient building block for such species in that it provides two differentiable tertiary amine sites at which quaternization can be performed to produce desired polycationic structures (Fig. 1A). Polycationic species derived from DABCO that possess a variety of interesting characteristics in biological systems and with molecules related to biological systems have previously been generated. For example, arrays of quaternized DABCO units along a linear aliphatic chain can modify the conformation of double stranded DNA (Cohen et al., 1999; Engel et al., 1999; Strekas et al., 1999). Quaternized DABCO units bound to cyclodextrins are capable of high-efficiency binding of amino acid and protein anion species (Cohen et al., 2000). Quaternized DABCO units bound to a cellulose surface can modify interactions with amino acid and protein species (Behaj et al., 2002). Finally, quaternized DABCO species bound to a variety of surfaces exhibit differentiable attack on bacterial and fungal cell walls to serve as antimicrobial surfaces (Fabian et al., 1997; Abel et al., 2002, 2003; Cohen and Engel, 2002; Cohen et al., 2004).

In this study, we showed that although nonsubstituted DABCO (1 mM) does not inhibit Kv2.1 or Kv3.4, submillimolar concentrations of various cell-safe substituted mono- and di-DABCO forms inhibit both channels with a range of IC_{50} values as low as 0.6 μM, whereas Kv4.2 channels are relatively insensitive. Block at an internal site on Kv2.1 was suggested against by the lack of effect of compounds applied via the recording electrode to Kv2.1 channels expressed in CHO cells. Voltage-dependence of block combined with mutagenesis and ability to protect from MTSET modification suggest DABCO-derived compounds block within the ion conduction pathway and that at least one binding site lies within the outer pore. These studies reveal that some DABCO derivatives are more effective blockers than any previously described quaternary ammonium ions, including TEA. Thus, DABCO derivatives represent a novel, diverse, and potent class of Kv channel blockers.

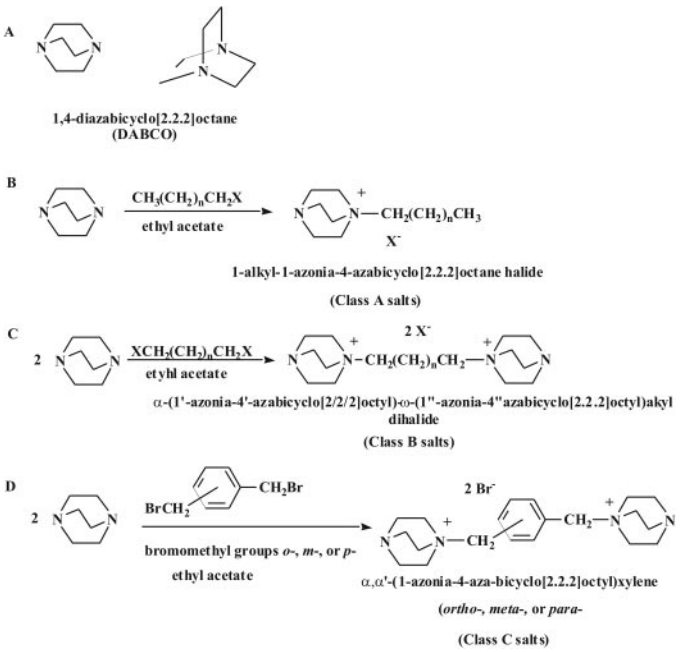

Fig. 1. Synthesis of representative DABCO derivatives. A, chemical structure of DABCO. B, synthesis of representative DABCO monostring. C, synthesis of representative diDABCO string. D, synthesis of representative aromatic diDABCO string.

Materials and Methods

Synthesis of DABCO Derivatives. DABCO (Fig. 1A) was purchased from Sigma-Aldrich Co. and used without further purification, as were the halogen-containing reagents. Modifications of prior reported synthesis procedures were used (Fabian et al., 1997; Cohen et al., 1999, 2000, 2004; Engel et al., 1999; Strekas et al., 1999; Abel et al., 2002, 2003; Behaj et al., 2002; Cohen and Engel, 2002). In general, DABCO was taken in reaction with a suitably functionalized haloalkane in an inert solvent (typically ethanol, unless limited reaction on the DABCO was desired, in which instances ethyl acetate was used). Three structural classes of DABCO derivatives were synthesized. Members of structural class A bear a lipophilic chain of variable length attached through one of the nitrogens of DABCO (Fig. 1B). Members of structural class B contain two DABCO units with a hydrocarbon spacer (Fig. 1C). Members of structural class C contain two DABCO units separated by carbon chains and an aromatic ring, with the substituents of the aromatic ring being in *ortho*, *meta*, and *para* relationships (Fig. 1D). For structures of type A, limited reaction of DABCO with a single equivalent of an appropriately substituted 1-haloalkane in ethyl acetate was performed followed by capping with the desired simple terminal haloalkane. For structures of type B, a diDABCO species was first generated by reaction of an excess of DABCO in ethyl acetate with the appropriate α,ω-dihaloalkane. The resultant material was then taken sequentially in limited reaction with a single equivalent of an appropriately substituted 1-haloalkane in ethyl acetate followed by capping with the desired simple terminal haloalkane. For structures of type C, an entirely analogous procedure was used as for the structures of type B, starting with the *ortho*-, *meta*-, and *para*-bis(halomethyl)benzene reagents. Compounds lacking detectable contaminants were adjudged pure with the use of NMR analysis.

Molecular Biology. Kv2.1 mutants were constructed using the QuikChange multi site-directed mutagenesis kit (Stratagene, La Jolla, CA). Mutant Kv2.1 genes (in the pGA1 oocyte expression vector for oocyte expression) were sequenced in their entirety to confirm appropriate mutations and to check for inadvertent mutations, and then subcloned into a wild-type pGA1 backbone. For oocyte expression, Kv3.4 was in pBF1 and Kv4.2 was in pRAT. cRNA transcripts were produced from SacII-linearized (Kv2.1), MluI-linearized (Kv3.4), and NotI-linearized (Kv4.2) DNA templates using the T3 (Kv2.1), SP6 (Kv3.4), and T7 (Kv4.2) mMessage mMachine kits (Ambion, Austin, TX). cRNA was quantified by spectrophotometry, and its size integrity was verified by gel electrophoresis. Defolliculated stage V and VI *Xenopus laevis* oocytes (purchased from Nasco, Grand Island, NY) were injected with 5 ng of cRNA encoding Kv2.1, Kv3.4, or Kv4.2. Chinese hamster ovary (CHO) cells were transfected with 0.25 μg of Kv2.1 cDNA, 2 μg of blank plasmid and 2 μg of green fluorescent protein in pBOB using *Superfect* transfec-

tion reagent (QIAGEN, Valencia, CA) 24 h before whole-cell, voltage-clamp studies.

Electrophysiology. Whole-cell two-electrode voltage-clamp (TEVC) recordings were performed on *X. laevis* oocytes expressing cloned Kv2.1, Kv3.4, or Kv4.2 using a OC-725C amplifier (Warner Instruments, Hamden, CT) and pClamp9 (Axon Instruments, Foster City, CA) software. Oocytes were bathed in a small-volume Warner oocyte bath and viewed with a dissection microscope (Fisher Scientific Co., Pittsburgh, PA). Bath solution for whole-cell oocyte recordings was 96 mM NaCl, 4 mM KCl, 0.7 mM $MgCl_2$, 1 mM $CaCl_2$, and 10 mM HEPES, pH 7.4; whole-cell oocyte TEVC pipettes were of 0.2- to 2-MΩ resistance when filled with 3 M KCl. Experiments were performed 24 to 48 h after cRNA injection. For assessment of current-voltage relationships in the absence or presence of DABCO derivatives, oocytes were held at −80 mV, stepped for 2 s at voltages between −80 mV and +60 mV in 20-mV steps (Kv2.1) or between −80 and +50 mV in 10-mV steps (Kv3.4), then held for 500 ms at −40 mV before returning to the holding potential (protocol 1). For assessment of block during wash-in of DABCO derivatives at a single voltage, oocytes were held at −80 mV and repetitively stepped to 0 mV for 2 s with an interpulse interval of 10 or 60 s as indicated (protocol 2). A range of concentrations of DABCO or DABCO derivatives were washed in via the bath solution during repetitive single-voltage pulses (after an initial period of five pulses with control solution to ensure current stabilization) until equilibrium block was achieved, to establish dose-responses. Inhibited currents are compared with the current at the end of five-pulse control period; thus, some bar graphs show "control" current values slightly less than 1 and with an error bar indicating to what extent currents deviate in the absence of drug. Washout was performed after the highest concentration of blocker was washed in. When washout was achieved, only those recordings in which current returned to within 10% of original current level were used for construction of dose-response curves. For cysteine protection experiments using the K356C variant of Kv2.1, a DABCO derivative (JC638.2α) was washed in to equilibrium block, followed by wash-in of a solution containing both JC638.2α and MTSET, until no further changes in current were seen; after this the solution was washed out with standard bath solution. As controls for this protection analysis, JC638.2α or MTSET were washed in alone until equilibrium block, then washed out.

For whole-cell voltage-clamp studies of CHO cells, bath solution was composed of 135 mM NaCl, 5 mM KCl, 1.2 mM $MgCl_2$, 5 mM HEPES, 2.5 mM $CaCl_2$, and 10 mM D-glucose, pH 7.4. Pipettes had resistances of 3 to 5 MΩ when filled with intracellular solution containing 10 mM NaCl, 117 mM KCl, 2 mM $MgCl_2$, 11 mM HEPES, 11 mM EGTA, and 1 mM $CaCl_2$, pH 7.2. For experiments with extracellular drug application, cells were held at −80 mV and subjected to 2-s test pulses from to 0 mV every 30 s. Whole-cell patch clamp recordings were performed at 22 to 25°C using an IX50 inverted microscope equipped with epifluorescence optics for GFP detection (Olympus, Tokyo, Japan), a Multiclamp 700A Amplifier, a Digidata 1300 Analog/Digital converter, and pClamp9 software (Axon Instruments). Leak and liquid junction potentials (<4 mV) were not compensated for when generating current-voltage relationships. For intracellular drug application, the tip of the recording electrode was first filled with drug-free intracellular solution, and the electrode was then back-filled with intracellular solution containing TEA (20 mM), TA279 (5 μM), or JC638.2α (0.5 mM). Cells were held at −80 mV and subjected to 2-s test pulses from −60 to +60 mV in 10-mV increments, followed by a 1-s tail pulse to −30 mV. After an initial recording, which we denoted time 0, a second recording was performed after 5 min.

Data Analysis. Current-voltage relationships were obtained by measuring peak current during depolarizing pulses. Inhibition constants for DABCO blockers were calculated after generating a dose-response curve by fitting with a logistic dose-response function $y = A_2 + [A_1 - A_2/1 + (x/x_0)^{n_H}]$, where A_1 is the maximum response plateau, A_2 is the minimum response plateau, x is drug concentration, x_0 is the IC_{50}, and n_H is the Hill slope. Data analysis was performed using Clampfit 9 (Axon Instruments, Foster City, CA) and tabulated in Excel 5.0 (Microsoft Corp., Redmond, WA). Graphs were generated using Origin 6.1 (OriginLab Corp, Northampton, MA). Data are expressed as mean ± S.E.M., with n specifying the number of independent experiments. Statistical significance was assessed by one-way ANOVA; $p < 0.05$ indicated significance.

Results

Kv2.1 and Kv3.4 Channels Are Differentially Inhibited by DABCO Monostrings. We initially explored blocking effects of nonsubstituted DABCO on Kv2.1 and Kv3.4 potassium channels. Kv2.1 is a delayed rectifier Kv channel expressed in mammalian heart, brain, and other excitable tissues. In particular, Kv2.1 facilitates dynamic control of neuronal excitability (Misonou et al., 2004), forms a component of the I_K cardiac myocyte repolarization current in rodent heart (Brunet et al., 2004), and generates an O_2-sensitive current in pulmonary arteries (Archer et al., 2004). Kv3.4 is a fast-inactivating Kv channel expressed primarily in the brain and skeletal muscle. Coassembly of Kv3.4 with delayed rectifier Kv3 subfamily α-subunits in the brain is thought to generate heteromeric channels with differing inactivation rates, perhaps enhancing firing rate of fast-spiking neurons (Baranauskas et al., 2003). In skeletal muscle, Kv3.4 forms complexes with the MiRP2 ancillary subunit to control myocyte excitability and repolarization (Abbott et al., 2001).

Bath-applied DABCO, at 1 mM, had no effect on the magnitude or kinetics of either Kv2.1 or Kv3.4 currents heterologously expressed in *X. laevis* oocytes, analyzed by TEVC (Fig. 2). Next, the sensitivities of Kv2.1 and Kv3.4 to two DABCO-derived monostrings, JE188 and TA279, were analyzed by functional expression in *X. laevis* oocytes using TEVC and bath application of the compounds at various concentrations.

The JE188 12-carbon monostring DABCO compound (Fig. 3A) significantly inhibited both Kv2.1 and Kv3.4 channels at 50 μM, with 250 μM producing almost complete inhibition in both cases (Fig. 3, B and C). Fitting of dose response curves with a logistic dose response function yielded JE188 inhibition constant IC_{50} values of 23.3 ± 2.1 and 34.2 ± 10 μM and slopes of 1.4 ± 0.1 and 0.7 ± 0.1 for Kv2.1 and Kv3.4, respectively (Fig. 3, D and E).

Recording of current-voltage "families" for both channel types in the presence and absence of JE188 showed voltage dependence of block in both cases such that inhibition was

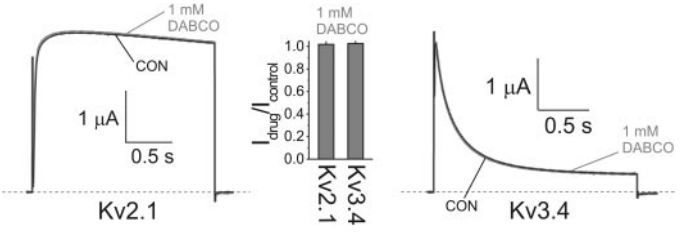

Fig. 2. 1,4-Diaza-bicyclo[2.2.2]octane (1 mM) does not affect Kv2.1 or Kv3.4 currents. Representative Kv2.1 (left) and Kv3.4 (right) traces recorded under control conditions and after perfusion with 1 mM DABCO. Currents were evoked by step depolarization to 0 mV (2 s) from a holding potential of −80 mV in oocytes heterologously expressing Kv2.1 or Kv3.4. Bar graph (center) shows the lack of effect of 1 mM DABCO on mean Kv2.1 and Kv3.4 current density. Error bars indicate S.E.M. (n = 3–4 oocytes).

much less pronounced at more positive voltages (Fig. 3, F and G). For Kv2.1 channels, mean inhibition was 3-fold more at 0 mV than at +60 mV (Fig. 3F); for Kv3.4 channels, mean inhibition was 2-fold more at 0 mV than at +50 mV (Fig. 3G). For Kv3.4 channels, crossover of the N-type inactivation occurred with application of 50 μM JE188, suggesting either slowing of inactivation or partial drug unbinding at depolarized voltages (Fig. 3C).

The TA279 16-carbon monostring DABCO compound (Fig. 4A) was the most potent compound we tested, inhibiting both Kv2.1 and Kv3.4 channels at 1 μM, with 5 μM producing almost complete inhibition in both cases (Fig. 4, B and C). Fitting of dose response curves with a logistic dose response function yielded IC_{50} values of 1.9 ± 3.6 and 0.6 ± 0.1 μM and slope values of 0.6 ± 0.4 and 2.8 ± 1.1 for Kv2.1 and Kv3.4, respectively (Fig. 4, D and E). These values indicate that Kv2.1 channels are 3000-fold more sensitive to block by externally applied TA279 than to block by externally applied TEA (Taglialatela et al., 1991), and Kv3.4 channels are 500-fold more sensitive (Schroter et al., 1991; Vega-Saenz de Miera et al., 1992). Block of Kv2.1 and Kv3.4 was again voltage-dependent; mean inhibition of Kv2.1 channels was 3-fold more at 0 mV than at +60 mV (Fig. 4F); for Kv3.4 channels, mean inhibition was 1.5-fold more at 0 mV than at +50 mV (Fig. 4G). For Kv3.4 channels, N-type inactivation was relatively less complete (as a proportion of peak current) in the presence of TA279 (Fig. 4C).

It is possible that externally applied TA279, unlike TEA, might cross the plasma membrane to access a higher-affinity internal site. TEA has a higher affinity site in the inner pore of Kv channels but can only access it when applied internally

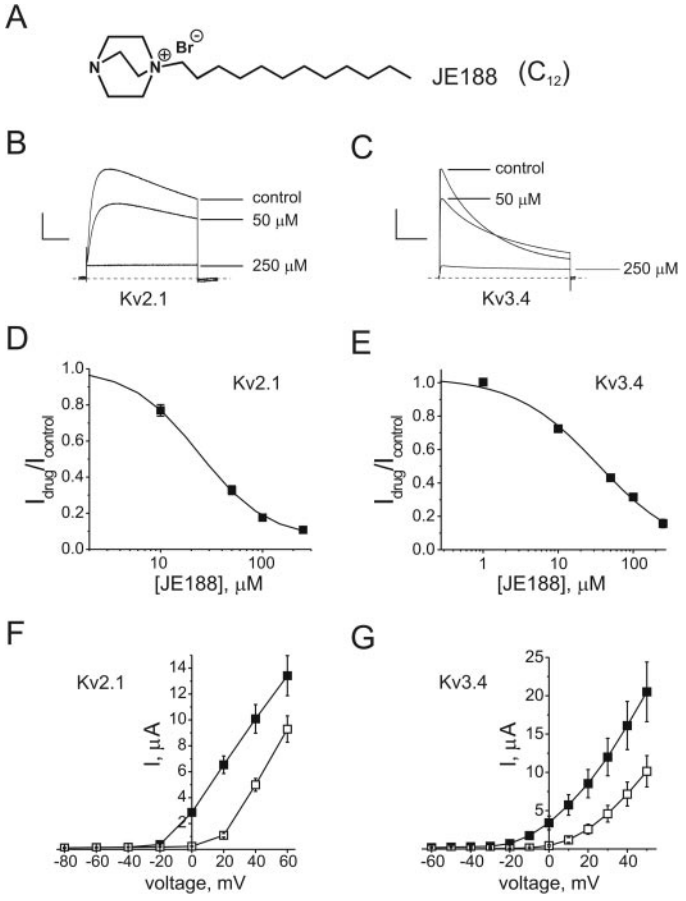

Fig. 3. JE188 inhibits Kv2.1 and Kv3.4. A, chemical structure of JE188. B, representative Kv2.1 current traces recorded under control conditions and after perfusion with JE188 (50 and 250 μM). Currents were evoked by step depolarizations to 0 mV (2 s) from a holding potential of −80 mV. Scale bars indicate 0.2 μA and 0.5 s. C, representative Kv3.4 current traces recorded under control conditions and after perfusion with JE188 (50 and 250 μM). Currents were evoked by step depolarizations to 0 mV (2 s) from a holding potential of −80 mV. Scale bars indicate 1 μA and 0.5 s. D, dose-response curve for the effect of JE188 on Kv2.1 peak currents. Error bars indicate S.E.M. (n = 5 oocytes). E, dose-response curve for the effect of JE188 on Kv3.4 peak currents. Error bars indicate S.E.M. (n = 5 oocytes). F, mean current-voltage relationship for oocytes expressing Kv2.1 under control conditions (■) or with 250 μM JE188 (□). Error bars indicate S.E.M. (n = 8 oocytes). G, mean current-voltage relationship for oocytes expressing Kv3.4 under control conditions (■) or with 250 μM JE188 (□). Error bars indicate S.E.M. (n = 5 oocytes).

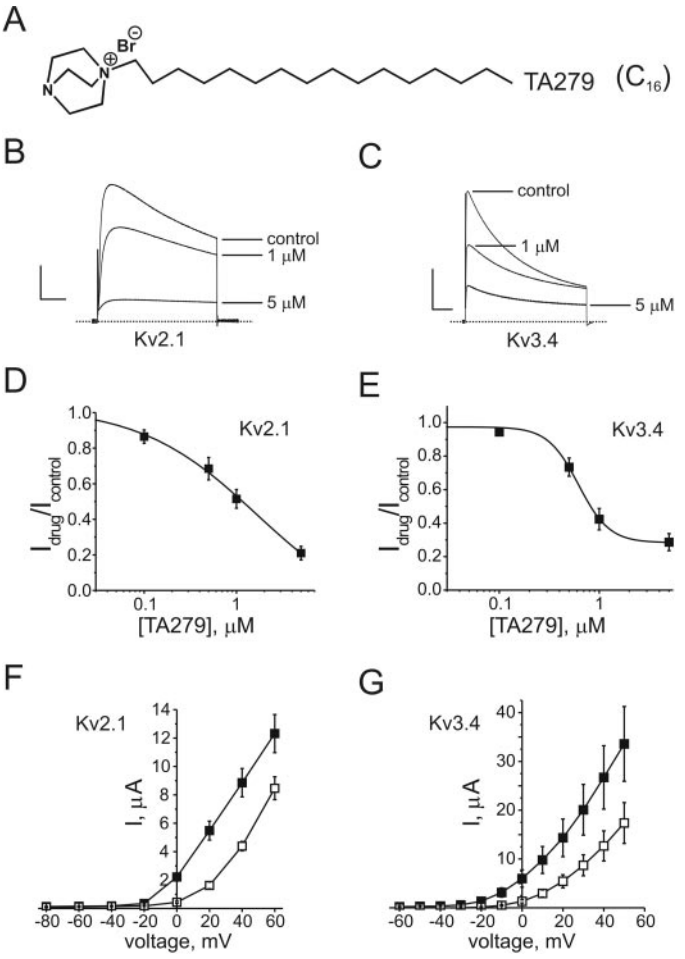

Fig. 4. TA279 inhibits Kv2.1 and Kv3.4. A, chemical structure of TA279. B, representative Kv2.1 current traces recorded under control conditions and after perfusion with TA279 (1 and 5 μM). Currents were evoked by step depolarizations to 0 mV (2 s) from a holding potential of −80 mV. Scale bars indicate 0.25 μA and 0.5 s. C, representative Kv3.4 current traces recorded under control conditions and after perfusion with TA279 (1 and 5 μM). Currents were evoked by step depolarizations to 0 mV (2 s) from a holding potential of −80 mV. Scale bars indicate 0.5 μA and 0.5 s. D, dose-response curve for the effect of TA279 on Kv2.1 peak currents. Error bars indicate S.E.M. (n = 6 oocytes). E, dose-response curve for the effect of TA279 on Kv3.4 peak currents. Error bars indicate S.E.M. (n = 5 oocytes). F, mean current-voltage relationship for oocytes expressing Kv2.1 under control conditions (■) or with 5 μM TA279 (□). Error bars indicate S.E.M. (n = 8 oocytes). ∗, significant difference between groups at −40 to +60 mV, $p < 0.005$. G, mean current-voltage relationship for oocytes expressing Kv3.4 under control conditions (■) or with 5 μM TA279 (□). Error bars indicate S.E.M. (n = 5 oocytes). ∗, significant difference between groups at −30 to +50 mV, $p < 0.05$.

(Armstrong, 1975). Indeed, TA279 washout was much slower than typically observed for TEA, taking several minutes, suggesting the possibility that it crosses the plasma membrane to exert its action. To assess at which side this DABCO derivative acted, TA279 was applied extracellularly (via the bath) and intracellularly (via the recording electrode) to Kv2.1 channels expressed in CHO cells. Extracellular application of 500 nM TA279 produced a mean current inhibition of 59 ± 4% at 0 mV (n = 3; Fig. 5A), indicating ~4-fold higher sensitivity than Kv2.1 channels expressed in oocytes, a common phenomenon because oocytes are thought to sequester some drugs, decreasing apparent sensitivity. Intracellular application of a 10-fold higher concentration of TA279 (5 μM) produced no significant block at 0 mV at 0 or 5 min after attaining the whole-cell configuration, compared with control currents in which no drug was added to the electrode, as assessed by one-way ANOVA (n = 4; Fig. 5, B and C). As a positive control, 20 mM TEA at 0 mV was shown to produce ~85% block at time 0 and ~88% block after 5 min. This essentially instantaneous intracellular block by TEA was reported previously using the same TEA concentration and technique (Immke et al., 1999). These data suggest that the high-affinity site of TA279 is accessed from outside the cell and does not require TA279 to cross the plasma membrane. The relatively slow washout of TA279 in oocytes may be due to sequestering of the drug in this system, a relatively common artifact.

Simple diDABCO strings, with a DABCO group at each end separated by a variable-length hydrocarbon chain (Fig. 6A), also inhibited both Kv2.1 and Kv3.4 channels but with lower affinity to the two monostrings tested. TG26 (4-carbon string) was less effective than TG27 (8-carbon string) at inhibiting either channel at a concentration of 1 mM; in the case of both compounds, Kv2.1 was more sensitive than Kv3.4 (Fig. 6, B–D). Construction of dose response curves yielded an IC_{50} for TG27 of 270.5 ± 66.4 μM and slope of 2.1 ± 0.8 for Kv2.1; Kv3.4 seemed somewhat less sensitive, but an accurate fit of the dose-response curve could not be achieved because application of TG27 at concentrations above 1 mM began to introduce nonspecific leak (Fig. 6, E and F). Likewise, construction of dose responses for TG26 was not possible because doses required to produce >50% block were toxic to the oocytes (data not shown).

Even greater differentiation between the potency of similar compounds for a given channel was observed with diDABCO compounds separated by an aromatic group. Three such compounds of similar structure except for the relative positioning of the DABCO groups on the aromatic were assessed: JSG17, TA37, and JC638.2α, which contain DABCO groups in *ortho*, *meta*, and *para* positions, respectively, around the central aromatic ring (Fig. 7 A). For both Kv2.1 and Kv3.4, only the

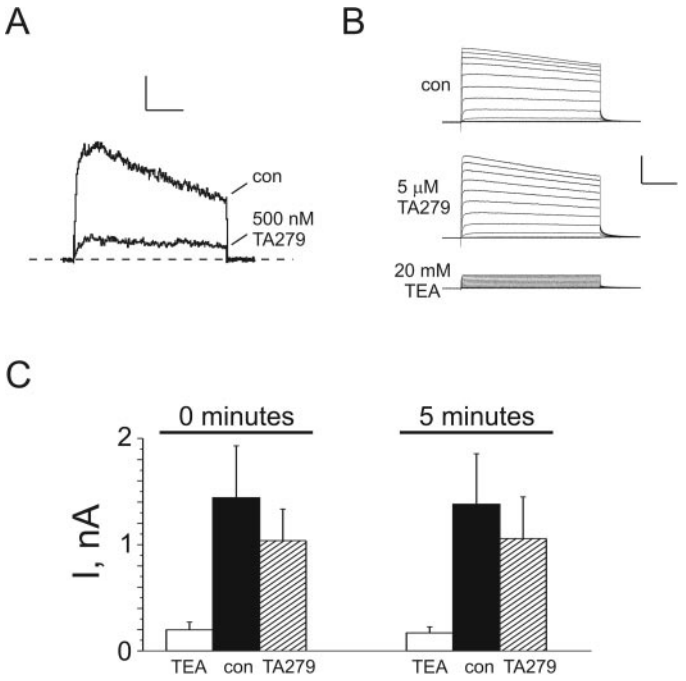

Fig. 5. TA279 acts at an external site on Kv2.1. A, exemplar traces recorded from a single CHO cell transfected with Kv2.1 cDNA. Currents were recorded at 0 mV before (con) or after external application to equilibrium block of 500 nM TA279 as indicated. Cells were held at −80 mV and pulsed to 0 mV every 30 s. B, exemplar traces recorded from CHO cells transfected with Kv2.1 cDNA. Currents were recorded with normal electrode solution (con) or solution containing 5 μM TA279 or 20 mM TEA, as indicated. Scale bars indicate 500 pA and 500 ms. Cells were held at −80 mV and pulsed to voltages between −60 mV and +60 mV in 10-mV increments for 2 s followed by a 1-s tail pulse. C, mean current densities for cells as in A, n = 4 cells per group. Error bars indicate S.E.M. Currents were recorded immediately after attainment of whole-cell configuration (0 min) or after 5 min as indicated. Groups are labeled according to composition of electrode solution, drug concentrations as in A.

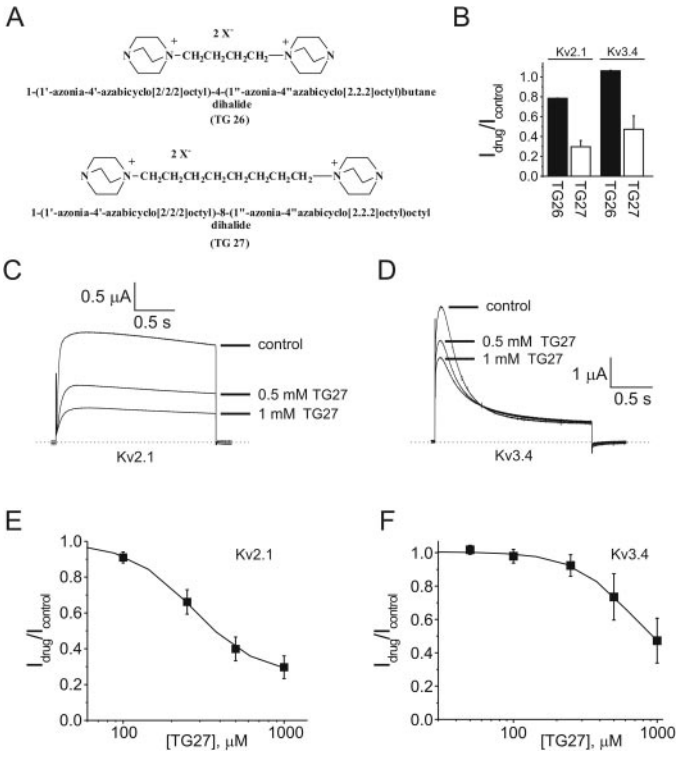

Fig. 6. diDABCO compounds inhibit Kv2.1 and Kv3.4. A, chemical structures of TG26 and TG27. B, bar graph showing the effect of 1 mM TG26 and TG27 on Kv2.1 and Kv3.4 currents. Error bars indicate S.E.M. (n = 3–10 oocytes). C, representative Kv2.1 current traces recorded under control conditions and after perfusion with TG27 (0.5 and 1 mM). Currents were evoked by step depolarization to 0 mV from a holding potential of −80 mV. Scale bars indicate 0.5 μA and 0.5 s. D, representative Kv3.4 current traces recorded under control conditions and after perfusion with TG27 (0.5 mM and 1 mM). Currents were evoked by step depolarization to 0 mV from a holding potential of −80 mV. Scale bars indicate 1 μA and 0.5 s. E, dose-response curve for the effect of TG27 on Kv2.1 peak currents. Error bars indicate S.E.M. (n = 10 oocytes). F, dose-response curve for the effect of TG27 on Kv3.4 peak currents. Error bars indicate S.E.M. (n = 3 oocytes).

para compound, JC638.2α, showed significant inhibition at 1 mM (Fig. 7B), indicating the critical nature of the shape of the compound in determining block. JC638.2α did not, however, significantly differentiate between Kv2.1 and Kv3.4 in terms of sensitivity (Fig. 7, C and D). Dose-response curves yielded IC_{50} values for JC638.2α of 185.7 $\pm$ 17 and 129 $\pm$ 20.7 μM and slope values of 1.4 $\pm$ 0.1 and 1.3 $\pm$ 0.2 for Kv2.1 and Kv3.4, respectively. As with the DABCO monostrings, JC638.2α showed voltage-dependent block, and inhibition was attenuated at more positive voltages (Fig. 7, E and F).

The sensitivity of Kv4.2, a fast-inactivating Kv channel with relatively low sensitivity to TEA compared with Kv2.1 and Kv3.4, was also screened for sensitivity to representative DABCO derivatives. Kv4.2 generates A-type currents in mammalian brain (Tsaur et al., 1992) and generates the cardiac I_{to} current in some species (Barry et al., 1995; Guo et al., 1999). As with previous reports for TEA (Blair et al., 1991), Kv4.2 was relatively insensitive to DABCO derivatives, showing 3% block with 100 μM JE188, 3% block with 1 mM TG27, and 38% block with 0.5 mM JC638.2α (Fig. 8). Thus, DABCO compounds, in particular simple monostrings and diDABCO strings, can be used to differentiate between transient outward currents generated by Kv3.4 versus Kv4.2 and at much lower concentrations than, for example, TEA. This property may prove useful in distinguishing between different A-type currents in brain regions in which both Kv3.4 and Kv4.2 are expressed, such as the hippocampus (Weiser et al., 1994; Martina et al., 1998).

JC.638.2α Binds at a Similar External Site to TEA in Kv2.1. Generation of current-voltage curves from families recorded in the presence or absence of DABCO-derived compounds such as JC638.2α indicated voltage dependence of block (Fig. 7, E and F). This may suggest that DABCO derivatives block within the ion conduction pathway, as observed for TEA. To explore this hypothesis further, we analyzed block of wild-type and mutant Kv2.1 channels by JC638.2α. First, we applied JC638.2α intracellularly to Kv2.1 channels expressed in CHO cells via the recording electrode. As with TA279, intracellularly applied JC638.2α (0.5 mM) produced no significant block at 0 mV compared with control recordings with no drug in the recording electrode, as assessed by one-way ANOVA (n = 4–5, Fig. 9, A and B), whereas in parallel positive control experiments, intracellularly applied TEA (20 mM) produced 70% and 80% block at 0 mV at 0 and 5 min, respectively (n = 3–5; Fig. 9B). This suggested that JC638.2α blocked via an external site rather than an internal site. According to some reports, Kv2.1 residue Tyr380 (equivalent to KcsA Tyr82 and *Shaker* Thr449) in the outer pore (Fig. 9C) forms at least part of the external TEA binding site (MacKinnon and Yellen, 1990; Heginbotham and MacKinnon, 1992; Luzhkov and Aqvist, 2001) although this has been subsequently disputed (Pascual et al., 1995; Crouzy et al., 2001; Andalib et al., 2004). The finding that Kv channels with an aromatic residue in this position are highly sensitive to block by external TEA was suggested to explain the higher TEA affinity of wild-type Kv2.1 compared with wild-type *Shaker* (MacKinnon and Yellen, 1990). The Y380T substitution in Kv2.1 reduces potency of block by external TEA; conversely, a T449Y mutation in *Shaker* enhances block by external TEA (50-fold) (Lipkind et al., 1995). In this study, we compared the effects of the Y380T mutation in Kv2.1 on block by JC.638.2α and found that the mutation did not alter block by JC638.2α, giving an IC_{50} of 185 $\pm$ 41 μM and a slope value of 1.3, not significantly different from wild-type (Fig. 9D). JC638.2α was chosen for these studies rather than the higher-affinity blocker TA279 because the relatively slow washout of TA279 rendered the next set of experiments impracticable.

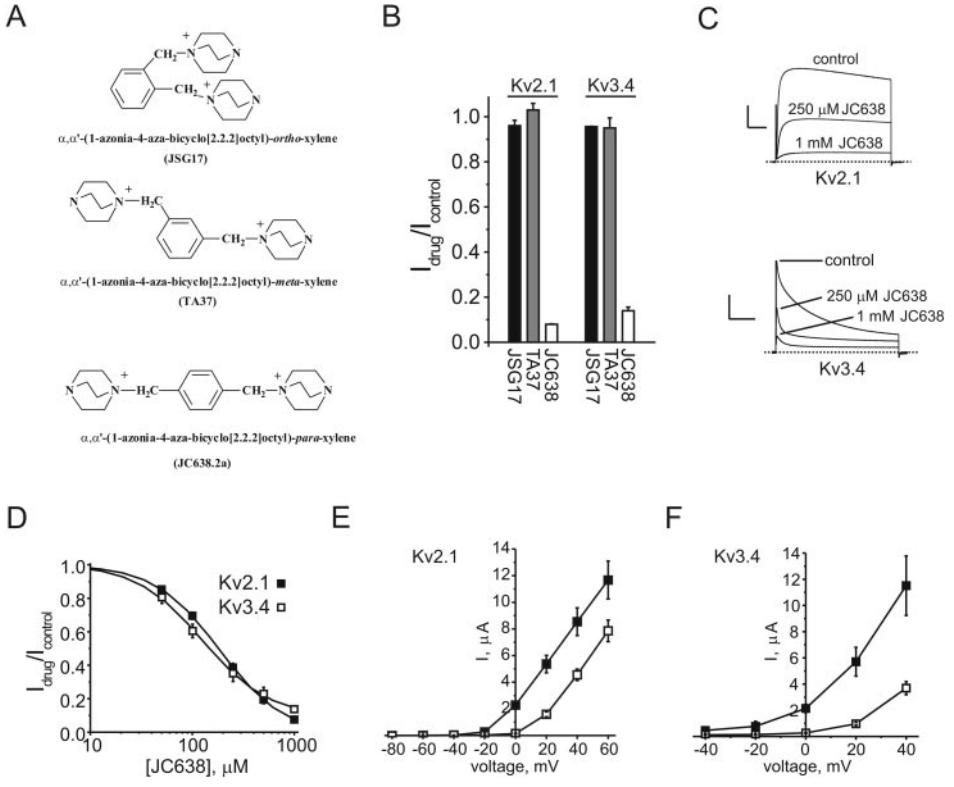

Fig. 7. Position of the DABCO group in aromatic compounds is critical for inhibition of Kv2.1 and Kv3.4. A, chemical structures of JSG17, TA37, and JC638.2α. B, bar graph showing the effect of 1 mM JSG17, TA37 and JC638.2α on Kv2.1 and Kv3.4 currents. Error bars indicate S.E.M. (n = 4–8 oocytes). C, representative Kv2.1 (top) and Kv3.4 (bottom) current traces recorded under control conditions and after perfusion with JC638.2α (0.25 and 1 mM). Currents were evoked by step depolarizations to 0 mV from a holding potential of −80 mV. Scale bars indicate 0.2 μA and 0.5 s (Kv2.1) or 0.5 μA and 0.5 s (Kv3.4). D, dose-response curve for the effect of JC638.2α on Kv2.1 (■) and Kv3.4 (□) peak currents. Error bars indicate S.E.M. (n = 5–10 oocytes). E, mean current-voltage relationship for oocytes expressing Kv2.1 under control conditions (■) or with 1 mM JC638.2α (□). Error bars indicate S.E.M. (n = 10 oocytes). F, mean current-voltage relationship for oocytes expressing Kv3.4 under control conditions (■) or with 1 mM JC638.2α (□). Error bars indicate S.E.M. (n = 5 oocytes).

Methanethiosulfonate forms the basis for a group of compounds that are able to bind irreversibly to the free sulfhydryl group of cysteine residues that line the pore of channels (Akabas et al., 1992; Karlin and Akabas, 1998). As was demonstrated by the Korn group (Andalib et al., 2004), introduction of a cysteine at position 356 in Kv2.1 made this position modifiable with MTSET, resulting in permanent fractional block. However, when TEA was administered before MTSET, this ability to permanently modify the introduced cysteine was lost. Thus, TEA protects Kv2.1 channels from MTSET modification, suggesting an external TEA binding site further from the pore than Kv2.1 residue K356, more distal from the pore than Tyr380 (Fig. 9C). Here, we investigated the ability of JC638.2α to prevent modification by MTSET at Kv2.1-K356C because of similarities between the effects of some DABCO compounds and TEA. When JC638.2α was administered alone, the K356C mutant was inhibited by 62 $\pm$ 3%; this block was reversed with washout (Fig. 9E). When MTSET was used to modify the introduced cysteine, currents

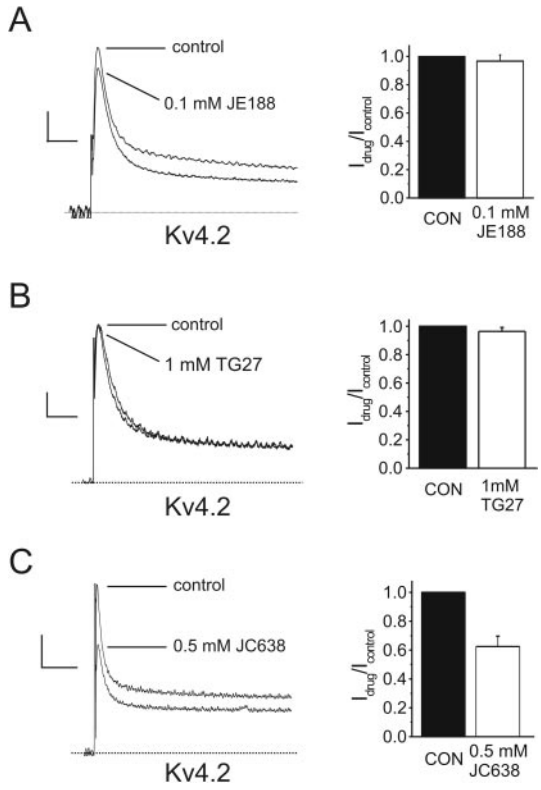

Fig. 8. Kv4.2 channels are relatively insensitive to DABCO compounds. A, left, representative heterologously expressed Kv4.2 current traces recorded in *X. laevis* oocytes under control conditions and after perfusion with 0.1 mM JE188. Currents were evoked by step depolarizations to 0 mV from a holding potential of −80 mV. Right, bar graph showing the mean effect of 0.1 mM JE188 on Kv4.2 currents. Error bars indicate S.E.M. (n = 7 oocytes). Scale bars indicate 0.2 μA and 60 ms. B, left, representative heterologously expressed Kv4.2 current traces recorded in *X. laevis* oocytes under control conditions and after perfusion with 1 mM TG27. Currents were evoked by step depolarizations to 0 mV from a holding potential of −80 mV. Right, bar graph showing the mean effect of 1 mM TG27 on Kv4.2 currents. Error bars indicate S.E.M. (n = 5 oocytes). Scale bars indicate 0.1 μA and 60 ms. C, left, representative heterologously expressed Kv4.2 current traces recorded in *X. laevis* oocytes under control conditions and after perfusion with 0.5 mM JC638.2α. Currents were evoked by step depolarizations to 0 mV from a holding potential of −80 mV. Right, bar graph showing the mean effect of 0.5 mM JC638.2α on Kv4.2 currents. Error bars indicate S.E.M. (n = 7 oocytes). Scale bars indicate 50 nA and 200 ms.

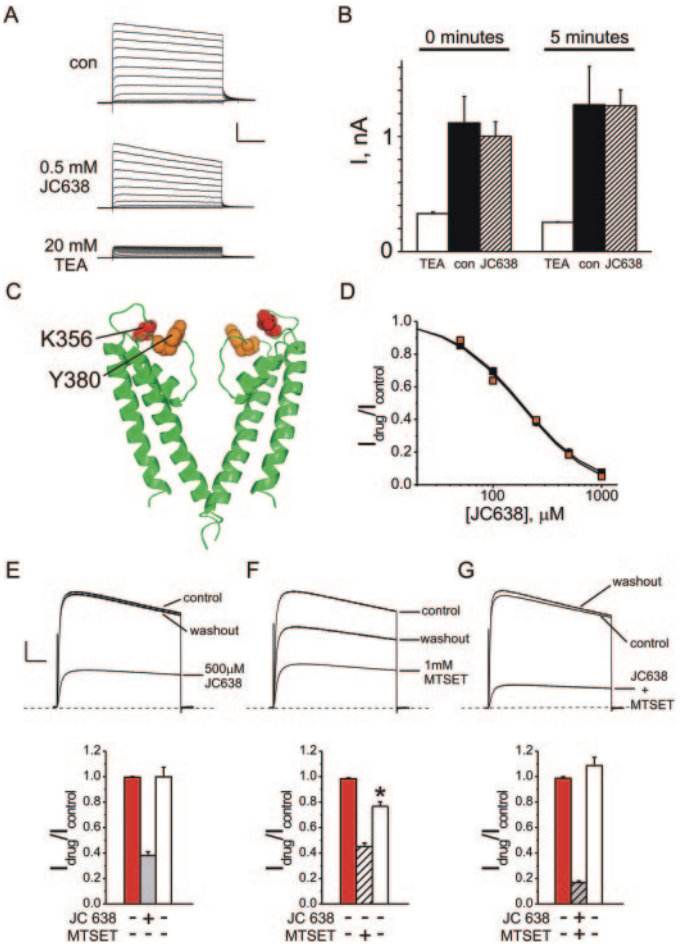

Fig. 9. A binding region for JC638.2α in the outer pore of Kv2.1. A, exemplar traces recorded from CHO cells transfected with Kv2.1 cDNA. Currents were recorded with normal electrode solution (con) or solution containing 0.5 mM JC638.2α or 20 mM TEA, as indicated. Scale bars indicate 500 pA and 500 ms. Cells were held at −80 mV and pulsed to voltages between −60 mV and +60 mV in 10-mV increments for 2 s followed by a 1-s tail pulse. B, mean current densities for cells as in A, n = 3–5 cells per group. Error bars indicate S.E.M.. Currents were recorded immediately after attainment of whole-cell configuration (0 min) or after 5 min as indicated. Groups are labeled according to composition of electrode solution, drug concentrations as in A. C, KcsA crystal structure with residues Gln58 (red) and Tyr82 (orange), equivalent to Kv2.1 Lys356 and Tyr380, respectively, highlighted. Two opposite subunits are shown with front and rear subunits removed for clarity. Coordinates from Doyle et al. (1998). D, dose-response curves for the effect of JC638.2α on wild-type (black squares) and Y380T (orange squares) Kv2.1 peak currents. Error bars indicate S.E.M. (n = 5–6 oocytes). E, top, representative traces; bottom, mean normalized currents; for K356C-Kv2.1 currents recorded in *X. laevis* oocytes in control solution (red bar) after perfusion with 500 μM JC638.2α (gray bar) and after washout of the drug (white bar). Currents were evoked by step depolarizations to 0 mV from a holding potential of −80 mV. Scale bars for E to G indicate 0.5 μA and 375 ms. Error bars indicate S.E.M. (n = 3 oocytes). F, top, representative traces; bottom, mean normalized currents; for K356C-Kv2.1 currents recorded in *X. laevis* oocytes in control solution (red bar) after perfusion with 2 mM MTSET (hatched bar) and after washout of the drug (white bar). Currents were evoked by step depolarizations to 0 mV from a holding potential of −80 mV. Error bars indicate S.E.M. (n = 3 oocytes). *, significant difference from control value after washout of MTSET, indicating incomplete reversibility of block by MTSET ($p < 0.05$). G, top, representative traces; bottom, mean normalized currents; for K356C-Kv2.1 currents recorded in *X. laevis* oocytes in control solution (red bar) after perfusion with a solution containing both 2 mM MTSET and 500 μM JC638.2α (hatched gray bar) and after washout of the two drugs (white bar). Currents were evoked by step depolarizations to 0 mV from a holding potential of −80 mV. Error bars indicate S.E.M. (n = 5 oocytes).

were inhibited 56 ± 3%; washout here was incomplete, leaving 24 ± 4% current inhibition remaining (Fig. 9F). Preapplication of JC638.2α prevented permanent modification of Kv2.1-K356C (Fig. 9G): coapplication of JC638.2α and MTSET inhibited K356C-Kv2.1 current by 84 ± 1%, completely reversible with washout. These effects are similar to those previously observed for protection from MTSET modification of Kv2.1-K356C by TEA, and together with the lack of effect of intracellularly applied JC638.2α, suggest that JC638.2α binds, like TEA, to a similar external site in Kv2.1.

Discussion

Kv channels are ubiquitously expressed in all excitable tissues and are targets or potential targets for pharmacologic therapies in disease states including cardiac arrhythmia, epilepsy, immune disorders, transplant organ rejection, deafness, cancer, hypertension, and stroke. There are 38 known Kv channel α-subunit genes, which can interact with a variety of regulatory subunits to generate a phenomenal diversity of native Kv currents (McCrossan and Abbott, 2004). The key to producing safe, efficacious drugs is to target specific channel Kv types to limit unwanted side effects. Advances in our understanding of the structure of potassium channels culminated recently in the determination of a high-resolution structure for Kv1.2, a mammalian Kv channel (Long et al., 2005a,b). Rational Kv channel structure-driven design of therapeutic drugs still requires much work, however, because the largely unknown subtle structural differences between channels such as Kv1.2 and its close relatives must be exploited for ultimate specificity.

Here, we reasoned that a polyammonium ion that permitted a range of chemical modifications might share the ability of TEA to block certain Kv channels but have the advantage of providing a platform for addition of diverse chemical groups to improve potency and specificity. The DABCO group provides two differentiable tertiary amine sites at which quaternization can be used to produced a wide array of different polycationic structures. Here, initial experiments using undifferentiated DABCO showed no effects on channel function, whereas quaternary DABCO-based compounds blocked Kv2.1 and Kv3.4 channels, leading to the conclusion that channel-blocking activity is directly related to introduction of one or more quaternary nitrogen groups. The active DABCO-based compounds are chemically similar to TEA in that they contain quaternary ammonium groups but display potencies significantly greater than TEA without losing relative specificity between different Kv channel subfamilies.

There was a distinct relationship between structure and activity of DABCO compounds, suggesting differences in accessibility to or affinity for discrete binding sites even between closely related compounds. The monostring compounds exhibited increasing affinity with increasing chain length, with TA279 (C_{16}) having an IC_{50} value 12 times lower that of JE188 (C_{12}). In diDABCO compounds with the functional moiety separated by a hydrocarbon linker, block was also dependent on the length of the interlinking chain. TG26 (C_4) had minimal effects on channel function, whereas TG27 (C_8) blocked Kv2.1 with an IC_{50} in the micromolar range. With all DABCO derivatives tested, block was voltage-dependent, with less extensive block at more positive voltages. Voltage dependence of block can suggest a binding site within the ion conduction pathway, or state dependence of block, or both (Clay, 1985). TEA exhibits voltage-dependent and state-dependent block of an internal binding site in Kv channels, but voltage-dependent, state-independent block when it binds to the external binding site (Armstrong, 1971; Thompson and Begenisich, 2003). Internal block of potassium channels by internally applied TEA and derivatives produces current decay resembling increased channel inactivation (Armstrong, 1969) but actually reflects the necessity for channel opening before block can occur (Armstrong, 1971). External block of Kv channels by TEA is voltage-dependent because of coupling with the movement of K^+ ions through the electrical field; the external TEA binding site itself is believed not to be far within the membrane electric field (Thompson and Begenisich, 2003). Because DABCO derivatives such as JE188 did not alter the apparent gating kinetics of Kv2.1, one might assume the block was not state-dependent and that the binding site probably lies within the ion conduction pathway. However, given the finding that affinity was increased with chain length of simple monostrings and di-DABCO strings, it is possible that these compounds bind to an external site on the channel but also cross the plasma membrane slowly to reach an internal site and gradually accumulate there—this eventuality, however, was suggested against by our finding that intracellular application of TA279 or JC638.2α did not produce block (Figs. 5 and 9). It is also possible that DABCO derivatives act in a similar fashion to some peptide toxins, such as hanatoxin, which inhibits Kv2.1 by binding to the voltage sensor (Wang et al., 2004). Again, this eventuality was suggested against by the mutagenesis studies in Fig. 9.

The relatively high affinities of Kv2.1 and Kv3.4 for compounds such as TA279, yet apparent absence of effect when applied intracellularly, suggest they bind with higher affinity than TEA to an external site but cannot block with high affinity the internal TEA site, which is a higher affinity site than the external site of Kv channels with regard to TEA (Armstrong, 1975). Thus, the apparent slowing of Kv3.4 inactivation by 50 μM JE188 (Fig. 3C) may actually reflect unbinding of the drug from the channel when we pulse to 0 mV, rather than being indicative of JE188 occupying the inactivation domain binding site within the inner pore, as was observed with tetrabutylantimony in KcsA using X-ray crystallography (Zhou et al., 2001). This unbinding would be consistent with the voltage-dependence of block by JE188, which shows greater block at more negative potentials (Fig. 3G).

In diDABCO compounds with an aromatic ring separating the two quaternary nitrogen groups, the position of the two side chains with respect to each other on the aromatic ring was found to be particularly crucial for block. Neither the (1,2)-*ortho* nor the (1,3)-*meta* di-substituted compounds blocked Kv2.1 or Kv3.4, but the (1,4)-*para* di-substituted compound did with IC_{50} values in the micromolar range. This probably reflects greater accessibility of the elongated *para* form to an external binding site, based on the mutagenesis and protection studies. This binding site is expected to be distal to the Tyr380 residue in Kv2.1 and interferes with MTSET modification of an introduced cysteine at K356. This finding is important because it should facilitate use of DABCO derivatives as probes of channel architecture in addition to aiding differentiation between different channel

populations in native preparations. In addition, these data (together with intracellular drug application studies from Figs. 5 and 9) assert that JC638.2α (and TA279) binds to an external site on Kv2.1. Thus, JC638.2α seems to bind near the Kv2.1 external TEA site with a 24-fold higher affinity than TEA, which has a reported IC_{50} of 4.5 mM with Kv2.1 (Immke et al., 1999). Exploitation of relatively small differences in channel architecture is crucial in the search for therapeutic agents that show specificity of action. Future studies will involve synthesis of a range of compounds similar to JC638.2α to test with a panel of Kv channels with the aim of exploiting structural differences in the outer pore to enhance specificity between closely related channels.

In summary, the discovery of the Kv channel blocking activity of DABCO-based compounds has defined a novel class of blockers that show a degree of specificity between Kv channel subfamilies, and relatively high potency compared with the related classic Kv channel blocker, TEA. As future synthesis strategies are guided by these initial findings, the key objectives will include development of compounds with increased specificity and potency, development of strategies to exploit DABCO compounds as probes of channel structure, and, ultimately, toxicity testing to explore the feasibility of therapeutic applications.

Acknowledgments

We are grateful to Dr. Valbona Behaj for valuable discussions at the inception of this project.

References

Abbott GW, Butler MH, Bendahhou S, Dalakas MC, Ptacek LJ, and Goldstein SA (2001) MiRP2 forms potassium channels in skeletal muscle with Kv3.4 and is associated with periodic paralysis. *Cell* **104:**217–231.

Abel T, Cohen JI, Engel R, Filshtinskaya M, Melkonian A, and Melkonian K (2002) Preparation and investigation of antibacterial carbohydrate-based surfaces. *Carbohydr Res* **337:**2495–2499.

Abel T, Cohen JI, Escalera J, Engel R, Filshtinskaya M, Fincher R, Melkonian A, and Melkonian K (2003) Polycations. 14. Preparation and investigation of protein-based antibacterial surfaces. *J Textile Apparel Tech Manage* **3:**1–8.

Akabas MH, Stauffer DA, Xu M, and Karlin A (1992) Acetylcholine receptor channel structure probed in cysteine-substitution mutants. *Science (Wash DC)* **258:**307–310.

Andalib P, Consiglio JF, Trapani JG, and Korn SJ (2004) The external TEA binding site and C-type inactivation in voltage-gated potassium channels. *Biophys J* **87:**3148–3161.

Archer SL, Wu XC, Thebaud B, Nsair A, Bonnet S, Tyrrell B, McMurtry MS, Hashimoto K, Harry G, and Michelakis ED (2004) Preferential expression and function of voltage-gated, O_2-sensitive K^+ channels in resistance pulmonary arteries explains regional heterogeneity in hypoxic pulmonary vasoconstriction: ionic diversity in smooth muscle cells. *Circ Res* **95:**308–318.

Armstrong CM (1969) Inactivation of the potassium conductance and related phenomena caused by quaternary ammonium ion injection in squid axons. *J Gen Physiol* **54:**553–575.

Armstrong CM (1971) Interaction of tetraethylammonium ion derivatives with the potassium channels of giant axons. *J Gen Physiol* **58:**413–437.

Armstrong CM (1975) Potassium pores of nerve and muscle membranes. *Membranes* **3:**325–358.

Baranauskas G, Tkatch T, Nagata K, Yeh JZ, and Surmeier DJ (2003) Kv3.4 subunits enhance the repolarizing efficiency of Kv3.1 channels in fast-spiking neurons. *Nat Neurosci* **6:**258–266.

Barry DM, Trimmer JS, Merlie JP, and Nerbonne JM (1995) Differential expression of voltage-gated K^+ channel subunits in adult rat heart. Relation to functional K^+ channels? *Circ Res* **77:**361–369.

Behaj V, Cohen JI, and Engel R (2002) Polycations. XI. Polycationic modified paper for chromatography. *Analyt Lett* **35:**1715–1720.

Blair TA, Roberds SL, Tamkun MM, and Hartshorne RP (1991) Functional characterization of RK5, a voltage-gated K+ channel cloned from the rat cardiovascular system. *FEBS Lett* **295:**211–213.

Brunet S, Aimond F, Li H, Guo W, Eldstrom J, Fedida D, Yamada KA, and Nerbonne JM (2004) Heterogeneous expression of repolarizing, voltage-gated K^+ currents in adult mouse ventricles. *J Physiol* **559:**103–120.

Clay JR (1985) Comparison of the effects of internal TEA^+ and Cs^+ on potassium current in squid giant axons. *Biophys J* **48:**885–892.

Cohen JI, Abel T, Burkett D, Engel R, Escalera J, Filshtinskaya M, Hatchett R, Leto M, Melgar Y, and Melkonian K (2004) Polycations. 15. Polyammonium surfaces—a new approach to antifungal activity. *Lett Drug Des Discov* **1:**88–90.

Cohen JI and Engel R (2002) Organic polycationic salts—syntheses and applications. *Curr Org Chem* **6:**1453–1467.

Cohen JI, Rusinowski A, Strekas TC, and Engel R (1999) Polycations. 6. Polycationic heterocyclic salts: their synthesis and effect on double stranded DNA. *Heteroatom Chem* **10:**559–565.

Cohen JI, Castro S, Han J-A, Shteto V, and Engel R (2000) Polycations. IX. Polyammonium derivatives of cyclodextrins—syntheses and binding to organic oxyanions. *Heteroatom Chem* **11:**546–555.

Crouzy S, Berneche S, and Roux B (2001) Extracellular blockade of K^+ channels by TEA: results from molecular dynamics simulations of the KcsA channel. *J Gen Physiol* **118:**207–217.

Doyle DA, Morais Cabral J, Pfuetzner RA, Kuo A, Gulbis JM, Cohen SL, Chait BT, and MacKinnon R (1998) The structure of the potassium channel: molecular basis of K^+ conduction and selectivity. *Science (Wash DC)* **280:**69–77.

Engel R, Shevchenko V, Lall S, Tropp B, Lau N, and Strekas T (1999) Synthesis and biological activities of phosphorus-containing polycationic strings. *Phosphorus Sulfur Silicon Relat Elements* **147:**83–84.

Fabian J, October T, Cherestes A, and Engel R (1997) Polycations: syntheses of polyammonium strings as antibacterial agents. *Synlett* **1997:**1007–1009.

Gulbis JM (2002) The beta subunit of Kv1 channels: voltage-gated enzyme or safety switch? *Novartis Found Symp* **245:**127–141; discussion 141–145; 165–168.

Guo W, Xu H, London B, and Nerbonne JM (1999) Molecular basis of transient outward K^+ current diversity in mouse ventricular myocytes. *J Physiol* **521:**587–599.

Heginbotham L and MacKinnon R (1992) The aromatic binding site for tetraethylammonium ion on potassium channels. *Neuron* **8:**483–491.

Heusser K and Schwappach B (2005) Trafficking of potassium channels. *Curr Opin Neurobiol* **15:**364–369.

Immke D, Wood M, Kiss L, and Korn SJ (1999) Potassium-dependent changes in the conformation of the Kv2.1 potassium channel pore. *J Gen Physiol* **113:**819–836.

Karlin A and Akabas MH (1998) Substituted-cysteine accessibility method. *Methods Enzymol* **293:**123–145.

Lipkind GM, Hanck DA, and Fozzard HA (1995) A structural motif for the voltage-gated potassium channel pore. *Proc Natl Acad Sci USA* **92:**9215–9219.

Long SB, Campbell EB, and Mackinnon R (2005a) Crystal structure of a mammalian voltage-dependent Shaker family K+ channel. *Science (Wash DC)* **309:**897–903.

Long SB, Campbell EB, and Mackinnon R (2005b) Voltage sensor of Kv1.2: structural basis of electromechanical coupling. *Science (Wash DC)* **309:**903–908.

Luzhkov VB and Aqvist J (2001) Mechanisms of tetraethylammonium ion block in the KcsA potassium channel. *FEBS Lett* **495:**191–196.

MacKinnon R (2003) Potassium channels. *FEBS Lett* **555:**62–65.

MacKinnon R and Yellen G (1990) Mutations affecting TEA blockade and ion permeation in voltage-activated K+ channels. *Science (Wash DC)* **250:**276–279.

Martina M, Schultz JH, Ehmke H, Monyer H, and Jonas P (1998) Functional and molecular differences between voltage-gated K^+ channels of fast-spiking interneurons and pyramidal neurons of rat hippocampus. *J Neurosci* **18:**8111–8125.

McCrossan ZA and Abbott GW (2004) The MinK-related peptides. *Neuropharmacology* **47:**787–821.

Misonou H, Mohapatra DP, Park EW, Leung V, Zhen D, Misonou K, Anderson AE, and Trimmer JS (2004) Regulation of ion channel localization and phosphorylation by neuronal activity. *Nat Neurosci* **7:**711–718.

Pascual JM, Shieh CC, Kirsch GE, and Brown AM (1995) K+ pore structure revealed by reporter cysteines at inner and outer surfaces. *Neuron* **14:**1055–1063.

Perozo E (2002) New structural perspectives on K^+ channel gating. *Structure (Camb)* **10:**1027–1029.

Rudy B, Chow A, Lau D, Amarillo Y, Ozaita A, Saganich M, Moreno H, Nadal MS, Hernandez-Pineda R, Hernandez-Cruz A, et al. (1999) Contributions of Kv3 channels to neuronal excitability. *Ann NY Acad Sci* **868:**304–343.

Strekas TC, Engel R, Locknauth K, Cohen J, and Fabian J (1999) Polycations. 5. Inducement of ψ-DNA circular dichroism signals for duplex deoxyribonucleotide homopolymers by polycationic strings. *Arch Biochem Biophys* **364:**129–131.

Thompson J and Begenisich T (2003) External TEA block of shaker K^+ channels is coupled to the movement of K^+ ions within the selectivity filter. *J Gen Physiol* **122:**239–246.

Tsaur ML, Sheng M, Lowenstein DH, Jan YN, and Jan LY (1992) Differential expression of K^+ channel mRNAs in the rat brain and down-regulation in the hippocampus following seizures. *Neuron* **8:**1055–1067.

Wang JM, Roh SH, Kim S, Lee CW, Kim JI, and Swartz KJ (2004) Molecular surface of tarantula toxins interacting with voltage sensors in K(v) channels. *J Gen Physiol* **123:**455–467.

Weiser M, Vega-Saenz de Miera E, Kentros C, Moreno H, Franzen L, Hillman D, Baker H, and Rudy B (1994) Differential expression of Shaw-related K^+ channels in the rat central nervous system. *J Neurosci* **14:**949–972.

Yellen G (2002) The voltage-gated potassium channels and their relatives. *Nature (Lond)* **419:**35–42.

Zhou M, Morais-Cabral JH, Mann S, and MacKinnon R (2001) Potassium channel receptor site for the inactivation gate and quaternary amine inhibitors. *Nature (Lond)* **411**:657–661.

Address correspondence to: Dr. Geoffrey W. Abbott, Starr 463, Greenberg Division of Cardiology, Weill Medical College of Cornell University, 520 East 70th Street, New York, NY 10021. E-mail: gwa2001@med.cornell.edu